Modelling the (Essential) Role of Proton Transport by Electrolyte Bases for Electrochemical Water Oxidation at Near-Neutral pH

Holger Dau * and **Chiara Pasquini**

Department of Physics, Free University Berlin, Arnimallee 14, 141595 Berlin, Germany;
chiara.pasquini@fu-berlin.de
* Correspondence: holger.dau@fu-berlin.de

Abstract: The oxygen-evolution reaction (OER) in the near-neutral pH-regime is of high interest, e.g., for coupling of OER and CO_2-reduction in the production of non-fossil fuels. A simple model is proposed that assumes equal proton activities in the catalyst film and the near-surface electrolyte. Equations are derived that describe the limitations relating to proton transport mediated by fluxes of molecular "buffer bases" in the electrolyte. The model explains (1) the need for buffer bases in near-neutral OER and (2) the pH dependence of the catalytic current at high overpotentials. The latter is determined by the concentration of unprotonated buffer bases times an effective diffusion constant, which can be estimated for simple cell geometries from tabulated diffusion coefficients. The model predicts (3) a macroscopic region of increased pH close to the OER electrode and at intermediate overpotentials, (4) a Tafel slope that depends on the reciprocal buffer capacity; both predictions are awaiting experimental verification. The suggested first-order model captures and predicts major trends of OER in the near-neutral pH, without accounting for proton-transport limitations at the catalyst–electrolyte interface and within the catalyst material, but the full quantitative agreement may require refinements. The suggested model also may be applicable to further electrocatalytic processes.

Keywords: electrocatalysis; mass transport limitation; oxygen-evolution reaction; OER

1. Introduction

The water oxidation reaction (or oxygen evolution reaction, OER) plays a key role in the global challenge towards the production of sustainable fuels [1–3]. In this framework, certain interesting applications require a catalyst that can be operated with reasonable efficiency in the neutral pH regime. Examples are the coupling of water oxidation with CO_2 reduction [4,5], the coupling of a photon absorber that can be corroded in extreme pH [6,7], and safety issues in home-localized devices [8,9]. However, operating the catalytic system at neutral pH can introduce mass-transport limitations, which are reported to prevent the development of efficient devices [10,11]. Local mass-transport limitation effects can be calculated based on the catalyst surface morphology [12]. The water oxidation reaction entails the release of four protons per each molecule of water produced. Thus, a high proton-transport capacity of the electrolyte is needed to prevent the formation of a local pH gradient. The choice of the electrolyte can strongly affect the catalytic performances [13] and has been the object of numerous literature studies [14–19]. In the Co oxide catalyst of the cobalt–phosphate type described first by Kanan and Nocera [20], we reported that the catalytic activity at high current density is proportional to the availability of unprotonated buffer molecules for a variety of tested buffer electrolytes [15]. The same has been observed for a Mn-based catalyst in phosphate buffer [21]. A related effect was observed for Mn-based catalysts where catalytic performances improved when the buffer pK_a was

increased, which has been attributed to a coupled proton–electron transfer mechanism between the catalyst and the buffer molecules [22]. Other studies, mostly based on analysis of CV experiments, suggest that the catalytic activity is mostly limited by the diffusion of the buffer molecules [23] or the protons [19] inside the bulk of the catalyst.

One of the most commonly used diagnostic tools in electrocatalysis is the study of the current-potential relation at steady-state (so-called Tafel plot). The interpretation of the data is often based on the Butler–Volmer equation [24,25]. The Tafel slope represents the increment in overpotential needed to obtain an increment of one decade in the current density; it is a key feature for assessment of catalyst efficiencies. Theoretical Tafel slope values have been derived for different water oxidation mechanisms [26] and for different rate-limiting steps [27]. Shinagawa et al. reported a large collection of experimental values for the Tafel slope. Only some of them can be explained by existing models [27]. Bediako et al. developed a model for bulk active catalysts at neutral pH and proposed various Tafel-slope values for different rate-controlling phenomena [28], e.g., diffusion of protons or buffer components inside the film or at the film–solution interface. Corresponding experiments on a CoO_x catalyst resulted in a Tafel slope of 59 mV dec^{-1} for high buffer concentrations and 118 mV dec^{-1} for buffer-free solutions, in accordance with their model predictions. In the intermediate cases, they predicted a transition between the two behaviors controlled by the buffer diffusion in solution. Here we present a model to describe the proton concentration in the electrolyte close to the catalyst in different currents and pH regimes, and its effect on catalytic activity and Tafel slope. Unconventional values for the Tafel slope and a strong local pH increase are predicted, inter alia furnishing a theoretical background to previous experimental findings [15].

2. Results

2.1. Outline of the Model

We are aiming at a simple model that describes the influence of proton transport mediated by buffer molecules on the catalytic activity. Therefore, we consider three regions (illustrated in Figure 1):

Region A: the (volume-active) OER catalyst film (Cat)—with its proton activity, X_{Cat}, and electric overpotential, ΔV.
Region B: a solvent layer (L) at the outer catalyst-film surface, the "buffer layer"—with its proton activity, X_{Layer}.
Region C: the bulk solvent (S)—with its proton concentration, c_H (pH = $-\log c_H$).

It is furthermore assumed that the effective proton concentrations, that is, *the proton activities in A and B are equal* once fluxes (of electrons and protons) and concentrations have reached a steady-state. Thus, they can be described by a single quantity, which in the following is denoted as X ($X_{Cat} = X_{Layer} = X$). This approximation reduces the number of effective compartments from three to two. The assumption is exact only if proton transport inside the catalyst film and proton transfer from the film to the solvent are kinetically not limiting; these processes are assumed to be clearly faster than the proton transport over macroscopic distances within the solvent phase.

The value of X determines both the rate of water oxidation within the catalyst and the rate of proton transfer from the buffer layer towards the bulk solvent. The proton transfer is mediated by protonation of a buffer base, which diffuses to the bulk solvent.
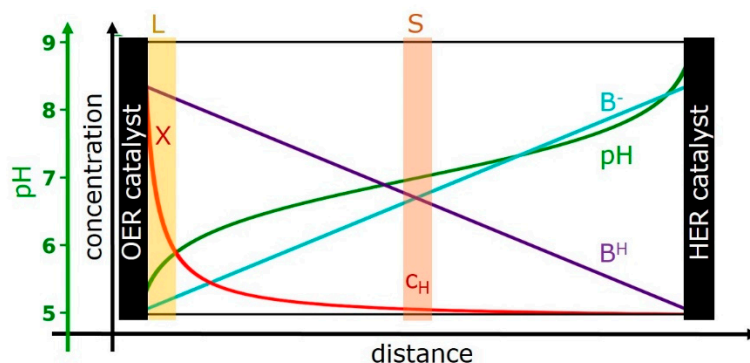
Figure 1. Cross-section of an idealized electrochemical cell with spatial concentration profiles of the protonated form of the buffer base (B^H, violet line), its deprotonated form (B^-, cyan line), and the proton concentration (red line). The corresponding pH profile also is indicated (green line). The scaling of the concentration axis for B^H and B^- differs from the scaling used for the proton concentration; a typical maximal B^H concentration would be in the range of 100 mM to 1 M (e.g., of phosphate buffer). The distance between the anode (oxygen-evolution reaction (OER) catalyst) and cathode (HER catalyst) could be, e.g., 1 cm. The OER catalyst is clearly thinner than drawn in the scheme, e.g., 500 nm. The "buffer layer" at the catalyst—solvent interface—is marked by L and highlighted by a yellow-brown area. The value of X provides the proton concentration or more precisely the proton activity directly at the surface of the OER catalyst. The proton concentration (activity) in the bulk solvent without any flow of catalytic currents is denoted as c_H. For operation at catalytic conditions, the proton concentration in the bulk solvent is equal to c_H only within a specific plane between anode and cathode, which is highlighted by a light-red area and marked by S. The shown concentrations profiles are an example; their form is in line with the proton transport model developed in the following, for an electrolyte filling the space between two parallel electrodes. In the shown example, we assume that c_H equals K_{aB} and corresponds to a pH of 7.

2.2. Catalytic Electron Flux

The quantity μ_x corresponds to the chemical potential of the protons within the catalyst film according to:

$$\mu_x = k_B T \ln X \tag{1}$$

It is now assumed that the catalytic electrical current (J_e) can be described by the following Butler–Vollmer type relation:

$$J_e = J_{e0} \exp \left[\alpha_{ET}(e\Delta V - \mu_x)/k_B T \right] \tag{2}$$

where ΔV, an electrical overpotential; J_{e0}, formal exchange current density; T, the temperature in Kelvin e, elementary charge; k_B, Boltzmann constant.

An alternative form of the above equation is used in the following ($\beta = e/K_B T$):

$$\ln J_e = \ln J_{e0} + \alpha_{ET} \beta \Delta V - \alpha_{ET} \ln X \tag{3}$$

Rearrangements lead to:

$$\Delta V = s_{ET} \ln J_e/J_{e0} + \beta^{-1} \ln X \tag{4}$$

with

$$s_{ET} = (\alpha_{ET} \beta)^{-1} \tag{5}$$

and X being a function of J_e ($X = X(J_e)$). The value of s_{ET} provides the so-called Tafel slope that is determined by α_{ET}, which depends on electrocatalytic properties (catalytic mechanisms and other properties) of the material. For example, an α_{ET} value of 1.0 corresponds to about 60 mV per decade (at room temperature); an α_{ET} value of 0.5 corresponds to about 120 mV per decade. The Tafel slope describes a linear relation between the applied electric potential and the logarithm ($\log_{10}$) of the current,

and it is often presented in units of mV per decade (of change in current density). The above value of s_{ET} relates to the natural logarithm; the classical decadic Tafel slope is obtained by:

$$s_{10\text{-}ET} = \ln 10 \; s_{ET} \tag{6}$$

The generalized definition of the Tafel slope is (based on the natural logarithm):

$$s = d \, \Delta V / d \ln J_e = s_{ET} + \beta^{-1} \, d \ln X(J_e)/d \ln J_e \tag{7}$$

The value of s_{ET} is the intrinsic Tafel slope of the catalyst material as it would be detectable in the absence of any limitations due to proton transport. Then X would be fully current-independent and equal to c_H; at room temperature the electric potential needed to maintain a given current would increase by about 60 mV per pH. Yet in the presence of proton-transport limitations, X is greater than c_H, and the magnitude of this difference increases with increasing current density (increasing J_e). Consequently, Equation (7) will provide Tafel slope values greater than s_{ET}.

2.3. Proton Flux Mediated by Buffer Molecules

The following considerations aim at relations between the proton activity of catalyst material and the adjacent buffer layer, X, and the magnitude of the proton flux, J_{BH}.

(1) The value of X determines the equilibrium between the protonated and the unprotonated buffer base of the electrolyte in the buffer layer at the catalyst surface according to:

$$B_L^- \, X / B_L^H = K_{aB} \tag{8}$$

Here B_L^- and B_L^H are the effective concentration (i.e., activity) of the unprotonated and protonated buffer base in the buffer layer, respectively. The value of K_{aB} relates to the pK_a value of the buffer ($-\log K_{aB} = pK_{aB}$).

With $B_0 = B_L^- + B_L^H$ we obtain:

$$B_L^H = B_0 \, X/(K_{aB} + X) \tag{9}$$

(2) In the bulk solvent (region C), the usual acid–base equilibrium prevails with a proton activity that corresponds to the bulk proton concentration (c_H, with pH = $-\log c_H$). Thus,

$$B_S^H = B_0 \, c_H/(K_{aB} + c_H) \tag{10}$$

B_S^- and B_S^H are the concentrations of the unprotonated base and protonated base in the bulk solution (i.e., far away from the catalyst surface), respectively. B_0 provides the total buffer concentration, which is the same in all three regions.

(3) The protonated and the unprotonated buffer are exchanged between the solvent layer and the bulk by means of diffusion, both described by the same effective diffusion constant, k_D. The flux of the proton-transporting base corresponds to a proton flux and, thus, a flux of positive charges, that is, a current. Thus, and for simplicity of the following considerations, the unit of choice for J_{BH} is A cm^{-2}. Accordingly, the B^H-flux from the buffer layer to the bulk solvent is described by (F, Faraday constant):

$$J_{BH}^{L=>S} = F \, dB_L^H/dt = k_D \, B_L^H \tag{11}$$

The B^H-flux from the bulk solvent to the buffer layer is described by

$$J_{BH}^{S=>L} = F \, dB_S^H/dt = k_D \, B_S^H \tag{12}$$

For continuous operation of the catalyst, a net flux of protons (J_{BH}) from the buffer layer to the solvent is mediated by diffusion of the protonated form of the buffer molecules that equals the difference between $J_{BH}^{S=>L}$ and $J_{BH}^{L=>S}$.

$$J_{BH} = J_{BH}^{L=>S} - J_{BH}^{S=>L} = k_D \, (B_L^H - B_L^S) \tag{13}$$

For continuous operation, the flux of unprotonated buffer molecules does not need to be considered explicitly because it matches the flux of the protonated buffer molecules. Moreover, it does not matter (for applicability of the above equations) how fast and where within the electrochemical cell the equilibrium distribution described by Equation (10) is reached. All details of the diffusion geometry and bulk-solvent equilibration are covered by the effective diffusion constant (k_D).

We note that Equation (13) can be understood in terms of Fick's first diffusion law: The diffusion flux is proportional to the concentration gradient; the diffusion coefficient, D (in m^2/s), is the proportionality constant. To illustrate the relation to Fick's law, we consider a particular simple electrode geometry: two parallel electrodes of identical area, the OER anode and the cathodic counter electrode, are located at a fixed distance, d_{el}, from each other; the unstirred electrolyte fills the volume exclusively in between of the two electrodes. Maintenance of a constant proton current mediated by diffusion of the protonated buffer base, B^H, requires a constant gradient of the B^H concentration; the B^H concentration equals B_L^H at the anode, $B_0 - B_L^H$ at the cathode, and B_L^S at an intermediate position between anode and cathode, as illustrated by Figure 1. Then the concentration gradient is given by $(B_L^H - B_L^S)/(d_{el}/2)$, and multiplication by D yields the proton flux in mol m^{-2} s^{-1}.

For the idealized electrode geometry, we obtain (F, Faraday constant):

$$k_D = F \, D/(d_{el}/2) \tag{14}$$

Using Equations (9)–(13), eventually we obtain:

$$J_{BH} = k_D \, B_0 \, [X/(K_{aB} + X) - c_H/(K_{aB} + c_H)] \tag{15}$$

Equation (15) implies that a maximal proton current density, J_{max}, exists for $X \gg K_{aB}$.

$$J_{max} = k_D \, B_0 \, [1 - c_H/(K_{aB} + c_H)] = k_D \, B_0 \, [K_{aB}/(K_{aB} + c_H)] \tag{16}$$

We note that J_{max} is not only proportional to the concentration of buffer molecules (B_0) and the effective diffusion constant (k_D) but is also pH-dependent. Since the last factor in Equation (16) provides exactly the fraction of unprotonated buffer molecules in the bulk solution, we can write Equation (16) also in the following form:

$$J_{max} = k_D \, B_0 \, [B_S^-/(B_S^- + B_S^H)] \tag{17}$$

Thus, J_{max} scales with the fraction of unprotonated buffer molecules.

Using Equation (16), rearrangement of Equation (15) yields:

$$X = [c_H + (J_{BH}/J_{max}) \, K_{aB}]/[1 - (J_{BH}/J_{max})] \tag{18}$$

For very small J_{BH} ($J_{BH} \ll J_{max}$), X equals c_H. Then the proton activity in buffer layer and catalyst (X) corresponds to the pH in the bulk electrolyte so that the local pH is very close to the bulk pH.

2.4. Current–Voltage Relation of OER Catalysis with Proton-Transport Limitations

For continuous operation of the electrocatalytic system (i.e., under steady-state conditions), the electric current density (J_e, Section 2.2) needs to be equal to the proton current density (J_{BH}, Section 2.3), which in the following is denoted by J:

$$J_e = J_{BH} = J \tag{19}$$

By means of Equation (4) and Equation (17) we obtain:

$$\Delta V = s_{ET} \ln J/J_{e0} + \beta^{-1} \ln \{[c_H + (J/J_{max}) K_{aB}]/[1 - (J/J_{max})]\} \tag{20}$$

with J_{max} according to Equation (16).

Figure 2 shows current–voltage relations for a buffer with a pK_a of 7 simulated based on Equation (20). At high potentials, the maximal current density, J_{max}, is reached.
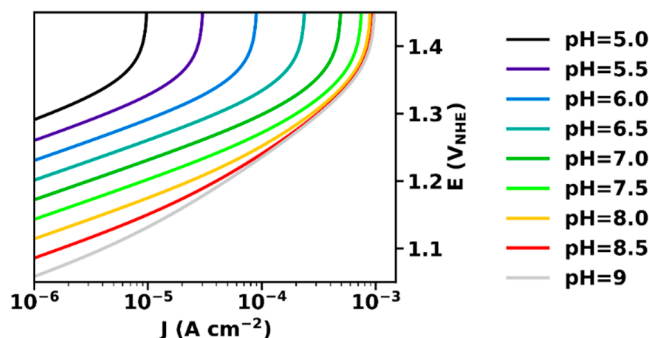

Figure 2. Current–voltage relation (Tafel-plots) at various pH, calculated according to Equation (20). The parameters used for simulation were: $\alpha_{ET} = 1$, $k_D = 10$ mA cm mol^{-1}, $B_0 = 0.1$ M, $pK_{aB} = 7$, $J_{e0} = 10^{-12}$ A cm^{-2}.

At low potentials and current densities, for $J \ll J_{max}$, we obtain from Equation (20):

$$\Delta V = s_{ET} \ln J/J_{e0} - \beta^{-1} pH \tag{21}$$

In this current regime, the slopes are equal to the intrinsic Tafel slope of the electrocatalyst material (s_{ET}, here assumed being 60 mV per decade), and the potential (vs. NHE) has a Nernstian dependence, i.e., decreases by 60 mV per pH unit.

At intermediate current densities, the slope is generally increased. This increase is minimal at pH 7 (for pH = pK_a) and more pronounced at higher and lower pH. This is seen more clearly in Figure 3, which shows the Tafel slope calculated by Equation (7).
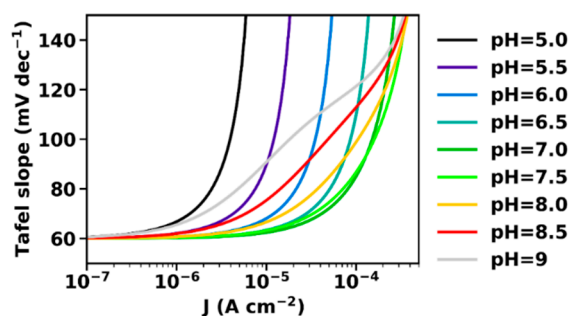

Figure 3. Tafel slopes at various pH, calculated according to the derivative of Equation (20). At low current densities at all investigated pH the Tafel slope is close to the "classical" value of 60 mV dec^{-1}, while at high current densities it increases due to proton transport limitations. The parameters used for simulation are the same also used in Figure 2: $\alpha_{ET} = 1$, $k_D = 10$ mA cm mol^{-1}, $B_0 = 0.1$ M, $pK_{aB} = 7$, $J_{e0} = 10^{-12}$ A cm^{-2}.

The maximal current density is determined by the concentration of the unprotonated buffer molecules and, thus, increases with increasing electrolyte pH. In clear contrast, the pH dependence of the Tafel slope at intermediate current densities is characterized by a minimum at the pK_a of the

buffer molecule. In the following, a rough approximation is presented that relates the Tafel slope to the capacity of the buffer molecules to stabilize the pH, i.e., the buffer capacity β_B.

Equation (7) implies for the total Tafel slope:

$$s = s_{ET} + s_{PT} \tag{22}$$

with

$$s_{PT} = \beta^{-1} \, d \ln X / d \ln J \tag{23}$$

We use the following identity:

$$d \ln X / d \ln J = (J/X) \, (dJ/dX)^{-1} \tag{24}$$

Substituting J by the expression derived in Section 2.3 for J_{BH} (Equation (15)) yields:

$$dJ/dX = K_D B_0 \, K_{aB}/(K_{aB} + X)^2 \tag{25}$$

and

$$s_{PT} = \beta^{-1} \, J \, [K_D B_0 \, K_{aB} \, X/(K_{aB} + X)^2]^{-1} \tag{26}$$

Using a highly approximative approach, we assume that X is close to c_H. For $X = c_H$, we obtain:

$$s_{PT} = \beta^{-1} \, J \, K_D / \beta_B \tag{27}$$

with

$$\beta_B = B_0 \, K_{aB} \, c_H / (K_{aB} + c_H)^2 \tag{28}$$

β_B is the pH-buffering capacity of the B^H/B^- buffer system of the electrolyte, which is maximal for $c_H = K_B$ (pH = pK_{aB}). Equation (27) correctly predicts the minimum of the Tafel slope at pH values close to the pK_a of the buffer molecules (Figure 4).
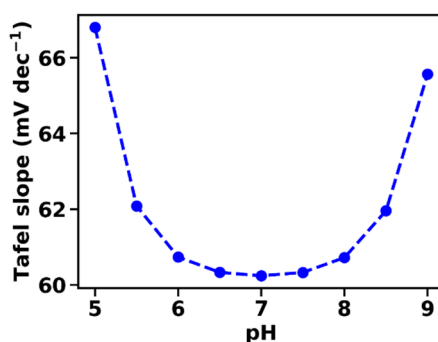

Figure 4. Tafel slopes at various pH extrapolated at 1 μA cm^{-2}, calculated according to the derivative of Equation (20). The pH dependence of the Tafel slope is closely related to the inverse of the buffer capacity of the electrolyte. The following parameters were used in the simulation: $\alpha_{ET} = 1$, $k_D = 10$ mA cm mol^{-1}, $B_0 = 0.1$ M, $pK_{aB} = 7$.

3. Discussion

In spite of its simplicity, the described model captures important aspects of the proton transport limitation in water oxidation at near-neutral pH.

In the absence of an explicit buffer base, either only water molecules or hydroxide ions can serve as proton-transporting buffer bases. Equation (15) shows that for H_2O molecules as proton acceptors, only minimal current densities can be reached in the neutral-pH region, because the local and bulk proton concentrations is, by many orders of magnitude, smaller than K_{aB} (for H_3O^+/H_2O, formal pK_{aB} of -1.74 or K_{aB} of 55 M); the J_{max} of Equation (16) can never be reached (because always X <<

K_{aB}). For OH^- ions as proton acceptors, their low concentration in the near-neutral pH regime results in an extremely small value of J_{max} in Equation (16) (for H_2O/OH^-, formal pK_{aB} of 15.74 or K_{aB} of 1.8×10^{-16}). For water oxidation in the acidic and alkaline pH regime, however, Equations (15) and (16) predict sizeable current densities. We note that for water or OH^- ion as proton acceptors, Equation (15) is no longer exact. At very low and very high pH, this equation becomes increasingly imprecise.

At high overpotentials, the catalytic current approaches a maximum value (J_{max} according to Equation (16)). Its pH dependence is determined by the concentration of unprotonated buffer molecules in the bulk electrolyte. This prediction has been verified by Klingan et al., where it was shown for nine buffer bases that the pH dependence of the current density at high overpotentials is determined by the protonation state of the respective buffer base [15].

At very low overpotentials, the catalytic current is not affected by proton transfer to the bulk electrolyte, but exclusively by the intrinsic electrocatalytic properties of the material. It is perfectly well described by a Tafel slope behavior with an increase in current density by a factor of 10 per pH unit at constant electric potential. At constant current density, a decrease in the required electric overpotential by $\ln(10) e/kT$ (about 60 mV at room temperature) per pH unit is predicted, as repeatedly observed in experimental studies [29–31].

At intermediate overpotentials, the Tafel slope increases in comparison to its low-overpotential value, which has been assigned before to mass transport limitations and largely can be avoided by the employment of a rotating-disc electrode [28,32–34]. In the described model, the mass transport limitations result from diffusion of protonated and unprotonated buffer bases in the electrolyte, without involving buffer base diffusion within the catalyst film. The diffusion process is described by an effective diffusion constant, k_D, per mol of buffer molecules. The use of a rotating disc electrode (or just stirring of the solution) would increase the value of k_D. The model predicts a macroscopic acidification in the electrolyte close to the catalyst surface, a prediction that still requires experimental verification. Moreover, the model predicts that at intermediate overpotentials the Tafel slope does not reflect the concentration of unprotonated buffer molecules, but rather the pH-buffering capacity of the B_H/B^- pH-buffer system (Equation (28), Figure 4). This dependence on an effective buffering capacity has not been reported before (to our best knowledge), and it, thus, represents another testable prediction of the presented model.

Application of the model in the extreme alkaline or acidic pH region (pH < 2 or pH > 12) also is possible, by substituting the unprotonated/protonated buffer base with the relevant water species: OH^-/H_2O at alkaline pH, H_2O/H_3O^+ at acidic pH. Then Equation (15) predicts sizeable current densities, inter alia because the diffusion coefficient (D) is about 10 times higher for H_3O^+ and five times higher for OH^- than for the commonly used buffer bases (e.g., $HPO_4^{2-}/H_2PO_4^-$). We note that for water or OH^- ion as proton acceptors, Equation (15) is no longer exact; at very low pH (<−1) and very high pH (>15) the imprecision will be sizable. At high current densities, the influence of Ohmic electrolyte conductivity and the associated electric field gradient is likely to result in further deviations from Equation (15). In any event, the here presented model is qualitatively in line with the long-standing finding that at elevated concentrations of OH^- or H_3O^+ ions, high current densities can also be ensured in the absence of an additional proton-accepting base, in clear contrast to the near-neutral pH regime,

4. Conclusions

The following phenomena are explained or predicted by the here developed model:

1. For pH values ranging from about 2 to 12, the OER reaction essentially requires buffer molecules that facilitate proton transport. In the absence of an explicit buffer base, either only water molecules or hydroxide ions could serve as proton-transporting buffer bases; both cannot support significant current densities.

2. In the presence of a buffer base, the maximal current density is determined by the concentration of unprotonated buffer molecules and, thus, by the solution pH and the pK_a value of the used buffer, in line with experimental findings [15].

3.　At intermediate current densities, the Tafel slope is increased in comparison to the intrinsic Tafel slope measured at low current densities. The Tafel slope increase is avoided only when macroscopic mass transport limitations are negligible, which is achievable experimentally, e.g., by employing catalyst films deposited on rotating disc electrodes. This behavior has been observed repeatedly and is, at least, qualitatively well explained by the presented model. Whether quantitative agreement with the here described first-order model can be reached is still unclear; extension of the model to include also (e.g.,) limitations of proton transport within the catalyst or at the catalyst–solvent interface may be required.

4.　At intermediate current densities, the Tafel slopes reflect the buffering capacity of the B^H/B^- couple, a prediction that still requires experimental verification.

5.　The limitations by proton transport are assigned to proton transport in the electrolyte phase. This assumption predicts (macroscopic) acidification of the electrolyte near the electrode surface, a prediction that still awaits experimental verification. Additional factors may contribute to proton transport limitations, specifically rate limitations by proton transfer at the catalyst–electrolyte interface or within the catalyst film. In the present model, these are excluded by assuming equal proton activities within the catalyst film and the near-surface electrolyte.

Author Contributions: Conceptualization, methodology, writing—original draft preparation, H.D.; validation, investigation, writing—review and editing, C.P.

Conflicts of Interest: The authors declare no conflict of interest.

References

1.　Hunter, B.M.; Gray, H.B.; Müller, A.M. Earth-Abundant Heterogeneous Water Oxidation Catalysts. *Chem. Rev.* **2016**, *116*, 14120–14136. [CrossRef] [PubMed]

2.　Roger, I.; Shipman, M.A.; Symes, M.D. Earth-abundant catalysts for electrochemical and photoelectrochemical water splitting. *Nat. Rev. Chem.* **2017**, *1*, 0003. [CrossRef]

3.　Lewis, N.S.; Nocera, D.G. Powering the planet: Chemical challenges in solar energy utilization. *Proc. Natl. Acad. Sci. USA* **2006**, *103*, 15729–15735. [CrossRef] [PubMed]

4.　Gattrell, M.; Gupta, N.; Co, A. A review of the aqueous electrochemical reduction of CO_2 to hydrocarbons at copper. *J. Electroanal. Chem.* **2006**, *594*, 1–19. [CrossRef]

5.　Jones, J.P.; Prakash, G.K.S.; Olah, G.A. Electrochemical CO_2 Reduction: Recent Advances and Current Trends. *Isr. J. Chem.* **2014**, *54*, 1451–1466. [CrossRef]

6.　Ismail, A.A.; Bahnemann, D.W. Photochemical splitting of water for hydrogen production by photocatalysis: A review. *Sol. Energy Mater. Sol. Cells* **2014**, *128*, 85–101. [CrossRef]

7.　Hisatomi, T.; Kubota, J.; Domen, K. Recent advances in semiconductors for photocatalytic and photoelectrochemical water splitting. *Chem. Soc. Rev.* **2014**, *43*, 7520–7535. [CrossRef]

8.　Nocera, D.G. Chemistry of personalized solar energy. *Inorg. Chem.* **2009**, *48*, 10001–10017. [CrossRef]

9.　Nocera, D.G. The artificial leaf. *Acc. Chem. Res.* **2012**, *45*, 767–776. [CrossRef]

10.　Jin, J.; Walczak, K.; Singh, M.R.; Karp, C.; Lewis, N.S.; Xiang, C. An experimental and modeling/simulation-based evaluation of the efficiency and operational performance characteristics of an integrated. *Energy Environ. Sci.* **2014**, *7*, 3371–3380. [CrossRef]

11.　McKone, J.R.; Lewis, N.S.; Gray, H.B. Will Solar-Driven Water-Splitting Devices See the Light of Day? *Chem. Mater.* **2014**, *26*, 407–414. [CrossRef]

12.　Suter, S.; Cantoni, M.; Gaudy, Y.K.; Pokrant, S.; Haussener, S. Linking morphology and multi-physical transport in structured photoelectrodes. *Sustain. Energy Fuels* **2018**, *2*, 2661–2673. [CrossRef]

13.　Shinagawa, T.; Takanabe, K. Towards Versatile and Sustainable Hydrogen Production through Electrocatalytic Water Splitting: Electrolyte Engineering. *ChemSusChem* **2017**, *10*, 1318–1336. [CrossRef] [PubMed]

14. Aiso, K.; Takeuchi, R.; Masaki, T.; Chandra, D.; Saito, K.; Yui, T. Carbonate Ions Induce Highly Efficient Electrocatalytic Water Oxidation by Cobalt Oxyhydroxide Nanoparticles. *ChemSusChem* **2017**, *10*, 687–692. [CrossRef] [PubMed]

15. Klingan, K.; Ringleb, F.; Zaharieva, I.; Heidkamp, J.; Chernev, P.; Gonzalez-Flores, D.; Risch, M.; Fischer, A.; Dau, H. Water oxidation by amorphous cobalt-based oxides: Volume activity and proton transfer to electrolyte bases. *ChemSusChem* **2014**, *7*, 1301–1310. [CrossRef] [PubMed]

16. Hunter, B.M.; Hieringer, W.; Winkler, J.R.; Gray, H.B.; Muller, A.M. Effect of interlayer anions on [NiFe]-LDH nanosheet water oxidation activity. *Energy Environ. Sci.* **2016**, *9*, 1734–1743. [CrossRef]

17. Surendranath, Y.; Dinca, M.; Nocera, D.G. Electrolyte-dependent electrosynthesis and activity of cobalt-based water oxidation catalysts. *J. Am. Chem. Soc.* **2009**, *131*, 2615–2620. [CrossRef]

18. Risch, M.; Klingan, K.; Ringleb, F.; Chernev, P.; Zaharieva, I.; Fischer, A.; Dau, H. Water oxidation by electrodeposited cobalt oxides—Role of anions and redox-inert cations in structure and function of the amorphous catalyst. *ChemSusChem* **2012**, *5*, 542–549. [CrossRef]

19. Brodsky, C.N.; Bediako, D.K.; Shi, C.; Keane, T.P.; Costentin, C.; Billinge, S.J.L.; Nocera, D.G. Proton–Electron Conductivity in Thin Films of a Cobalt–Oxygen Evolving Catalyst. *ACS Appl. Energy Mater.* **2018**, *1*, 1–2. [CrossRef]

20. Kanan, M.W.; Nocera, D.G. In situ formation of an oxygen-evolving catalyst in neutral water containing phosphate and Co^{2+}. *Science* **2008**, *321*, 1072–1075. [CrossRef]

21. Bergmann, A.; Zaharieva, I.; Dau, H.; Strasser, P. Electrochemical water splitting by layered and 3D cross-linked manganese oxides: Correlating structural motifs and catalytic activity. *Energy Environ. Sci.* **2013**, *6*, 2745–2755. [CrossRef]

22. Yamaguchi, A.; Inuzuka, R.; Takashima, T.; Hayashi, T.; Hashimoto, K.; Nakamura, R. Regulating proton-coupled electron transfer for efficient water splitting by manganese oxides at neutral pH. *Nat. Commun.* **2014**, *5*, 4256. [CrossRef] [PubMed]

23. Costentin, C.; Porter, T.R.; Saveant, J.-M. Conduction and Reactivity in Heterogeneous-Molecular Catalysis: New Insights in Water Oxidation Catalysis by Phosphate Cobalt Oxide Films. *J. Am. Chem. Soc.* **2016**, *138*, 5615–5622. [CrossRef] [PubMed]

24. Bard, A.J.; Faulkner, L.R. *Electrochemical Methods. Fundamentals and Application*; Wiley: Hoboken, NJ, USA, 1980.

25. Fletcher, S. Tafel slopes from first principles. *J. Solid State Electrochem.* **2009**, *13*, 537–549. [CrossRef]

26. Bockris, J.O.; Otagawa, T. Mechanism of oxygen evolution on perovskites. *J. Phys. Chem.* **1983**, *87*, 2960–2971. [CrossRef]

27. Shinagawa, T.; Garcia-esparza, A.T.; Takanabe, K. Insight on Tafel slopes from a microkinetic analysis of aqueous electrocatalysis for energy conversion. *Sci. Rep.* **2015**, *5*, 13801. [CrossRef] [PubMed]

28. Bediako, D.K.; Costentin, C.; Jones, E.C.; Nocera, D.G.; Savéant, J.-M. Proton–Electron Transport and Transfer in Electrocatalytic Films. Application to a Cobalt-Based O_2-Evolution Catalyst. *J. Am. Chem. Soc.* **2013**, *135*, 10492–10502. [CrossRef]

29. Surendranath, Y.; Kanan, M.W.; Nocera, D.G. Mechanistic studies of the oxygen evolution reaction by a cobalt-phosphate catalyst at neutral pH. *J. Am. Chem. Soc.* **2010**, *132*, 16501–16509. [CrossRef]

30. Zaharieva, I.; Chernev, P.; Risch, M.; Klingan, K.; Kohlhoff, M.; Fischer, A.; Dau, H. Electrosynthesis, functional and structural characterization of a water-oxidizing manganese oxide. *Energy Environ. Sci.* **2012**, *5*, 7081–7089. [CrossRef]

31. Huynh, M.; Bediako, D.K.; Nocera, D.G. A Functionally Stable Manganese Oxide Oxygen Evolution Catalyst in Acid. *J. Am. Chem. Soc.* **2014**, *136*, 6002–6010. [CrossRef]

32. Ullman, A.M.; Brodsky, C.N.; Li, N.; Zheng, S.-L.; Nocera, D.G. Probing Edge Site Reactivity of Oxidic Cobalt Water Oxidation Catalysts. *J. Am. Chem. Soc.* **2016**, *138*, 4229–4236. [CrossRef] [PubMed]

33. Low, C.T.J.; Ponce de Leon, C.; Walsh, F.C. The Rotating Cylinder Electrode (RCE) and its Application to the Electrodeposition of Metals. *Aust. J. Chem.* **2005**, *58*, 246–262. [CrossRef]

34. Schmidt, T.J.; Gasteiger, H.A.; Stäb, G.D.; Urban, P.M.; Kolb, D.M.; Behm, R.J. Characterization of High-Surface-Area Electrocatalysts Using a Rotating Disk Electrode Configuration. *J. Electrochem. Soc.* **1998**, *145*, 2354–2358. [CrossRef]